JOURNAL OF MATERIALS SCIENCE 35 (2000) 863–872

Oxidation behavior of $Mo_{\leq 5}Si_3C_{\leq 1}$ and its composites

Q. ZHU, K. SHOBU, E. TANI, K. KISHI, S. UMEBAYASHI
Kyushu National Industrial Research Institute, 841-0052, Japan
E-mail: zhu@kniri.go.jp

The oxidation behavior of $Mo_{\leq 5}Si_3C_{\leq 1}$ and its composites was studied in air over the temperature range of 500°C–1600°C. Experiments revealed poor oxidation resistance of monolithic $Mo_{\leq 5}Si_3C_{\leq 1}$ at high temperature. The oxidation was quite rapid at 1200°C and above, resulting in complete oxidation of specimens in a short time. The addition of 2.0 wt% boron was found to produce a $Mo_{\leq 5}Si_3C_{\leq 1}$ composite with three other phases of MoB, $MoSi_2$, and SiC, and showed remarkable improvement in oxidation resistance. The mechanism for the improvement was attributed to the viscous sintering of the scale to close the pores formed during the initial oxidation period. Oxidation tests were also conducted on SiC-$Mo_{\leq 5}Si_3C_{\leq 1}$ composite at 800°C, 1300°C and 1600°C for more than 100 hours. The oxidation resistance of the composite was found to be very good. The results demonstrate that, though oxidation resistance of monolithic $Mo_{\leq 5}Si_3C_{\leq 1}$ is far insufficient for high-temperature applications, boron-modification and/or composites with SiC are viable methods to improve oxidation resistance to a practically acceptable level.

1. Introduction

For structural applications in high-temperature environments, a material should have adequate strength, creep resistance and oxidation resistance [1, 2]. Among various advanced materials that are being studied for high-temperature applications, composites based on the Mo-Si-C system are of interest as envisaged by $MoSi_2$ and SiC with a high melting point and good oxidation resistance at high temperature. Although $MoSi_2$ shows excellent oxidation resistance at high temperature, monolithic $MoSi_2$ exhibits only modest value of fracture toughness [3, 4] at room temperature and has a high creep rate [5, 6] above 1200°C, making it unsuitable as a high-temperature structural material. Molybdenum carbosilicide ($Mo_{\leq 5}Si_3C_{\leq 1}$) is another interesting material in the Mo-Si-C system, because it (1) has a high melting point of around 2100°C, (2) has relatively complex crystal structure that may lead to better creep resistance, and (3) it is the only stable ternary phase in the Mo-Si-C system. Therefore, it is chemically compatible with SiC, C and $MoSi_2$ at high temperature.

Since the first detailed study on the ternary Mo-Si-C system by Nowotny *et al*. [7], several researches have been undertaken on the Mo-Si-C system and the $Mo_{\leq 5}Si_3C_{\leq 1}$ phase [8–11]. $Mo_{\leq 5}Si_3C_{\leq 1}$ was found in hot-pressed (HP) $MoSi_2$ compact when carbon was used as the deoxidant to remove SiO_2 at grain boundaries, and the presence of $Mo_{\leq 5}Si_3C_{\leq 1}$ was suggested to improve the mechanical properties of the $MoSi_2$ compact [12, 13]. Costa e Silva and Kaufman [11] demonstrated that the third phase in silicon-lean $MoSi_2$-SiC composites should be $Mo_{\leq 5}Si_3C_{\leq 1}$ instead of Mo_5Si_3. Recently, monolithic $Mo_{\leq 5}Si_3C_{\leq 1}$ compacts were synthesized by Suzuki and Niihara [14] through the HP method. The authors suggested that $Mo_{\leq 5}Si_3C_{\leq 1}$ could be used as a new matrix material as well as second-phase reinforcement material for high-temperature applications. Although significant attention has been paid to $Mo_{\leq 5}Si_3C_{\leq 1}$, most properties of the material are still unknown, for example, the oxidation resistance has not been clarified, which is often the primary criterion [15] in the selection of structural materials for high-temperature applications.

The purpose of the present study is to explore the oxidation behavior of $Mo_{\leq 5}Si_3C_{\leq 1}$. High-density monolithic $Mo_{\leq 5}Si_3C_{\leq 1}$ was synthesized by the HP method, and the oxidation behavior of monolithic $Mo_{\leq 5}Si_3C_{\leq 1}$ was investigated from 500°C to 1300°C in air. Boron addition was examined to improve the oxidation resistance of $Mo_{\leq 5}Si_3C_{\leq 1}$, and the oxidation resistance of B-$Mo_{\leq 5}Si_3C_{\leq 1}$ was tested up to 1500°C. Oxidation tests were also conducted on SiC-$Mo_{\leq 5}Si_3C_{\leq 1}$ composites fabricated by the melt infiltration process.

2. Experimental procedure

2.1. Sample preparation

Monolithic $Mo_{\leq 5}Si_3C_{\leq 1}$ was synthesized from raw powders of $MoSi_2$ (circa 1 μm, Japan New Metals, 99.94%), SiC (α, circa 3.2 μm, Showa Denko, Japan, 99%) and Mo (circa 1.3 μm, Japan New Metals, 99.9%). The powders were mixed by wet ball milling in alcohol for 3 hours, followed by drying in an oven.

The mixture was then packed into a graphite die coated with BN, followed by HP under an applied pressure of 15 to 35 MPa at 1500°C to 1700°C for 1 to 3 hours. The resultant disks were 12 mm in diameter and about 6 mm in thickness. Approximately 1mm was ground out from each surface of the disk to eliminate the region affected by the proximity of the die. The disk was then cut and ground into small specimens with 4 mm × 3 mm × 2 mm dimensions, followed by polishing with 1 μm diamond paste. Boron-doped $Mo_{\leq 5}Si_3C_{\leq 1}$ compacts, containing 2.0 wt% B, were also prepared by the same procedure using the raw powder of B (circa 1 μm, Furuwaki Chemical, Japan, 99%). The material will be subsequently termed B-$Mo_{\leq 5}Si_3C_{\leq 1}$.

SiC-$Mo_{\leq 5}Si_3C_{\leq 1}$ composites were fabricated by the melt infiltration process. A 40 × 16 × 6 (mm) preform was prepared by molding SiC raw powder in a die and then pressed by a cold isostatic press (CIP) under 300 MPa. The relative density of the preform was estimated to be around 70%. The infiltrant was the same mixture as that used for the fabrication of monolithic $Mo_{\leq 5}Si_3C_{\leq 1}$. The infiltration was performed at 2100°C for 10 minutes in flowing argon using an induction furnace.

2.2. Properties evaluation and oxidation tests

The microstructure of $Mo_{\leq 5}Si_3C_{\leq 1}$ and its composites was characterized by optical microscopy and scanning electron microscopy (SEM). An energy-dispersive X-ray spectrometer (EDS) was used to determine the composition of these materials. The crystalline phases were evaluated by an X-ray diffractometer (XRD). The density of the samples was determined by Archimedes' principle using water. Thermogravimetric analyses were carried out (Shimadzu, DT-300, Japan) under natural convection conditions in air between 500°C to 1300°C. The mass change was continuously recorded by a personal computer. Oxidation tests above 1300°C were conducted in air using a high-temperature thermal analysis system (Thermal Analysis Station, TAS 100, Rigaku Corp., Japan).

3. Results and discussion

3.1. Materials synthesis

The composition of $Mo_{45}Si_{30}C_5$ was selected as the initial composition, because it was reported [14] that near this composition single phase $Mo_{\leq 5}Si_3C_{\leq 1}$ was easily obtained. The fabrication of monolithic $Mo_{\leq 5}Si_3C_{\leq 1}$ compacts was first attempted by melting the mixture at 2100°C in an induction furnace, followed by solidification. Although the melting of the mixture was observed at around 2030°C, it was difficult to obtain a dense $Mo_{\leq 5}Si_3C_{\leq 1}$ material. The microstructure was not homogenous with many voids, pores and possibly other phases (carbon, SiC and/or $MoSi_2$) even when re-melting was performed several times at 2100°C.

Accordingly, monolithic $Mo_{\leq 5}Si_3C_{\leq 1}$ was synthesized by hot pressing at temperatures from 1500°C to 1700°C. Single-phase $Mo_{\leq 5}Si_3C_{\leq 1}$ could be obtained only when the sintering time was more than one hour; otherwise, $MoSi_2$, SiC or carbon phases may remain in the microstructure. Also, the pressure of 15 MPa was insufficient to obtain a fully dense compact even at 1800°C; a pressure of 35 MPa was necessary to achieve a density over 95% of theoretical density. The density of the samples consolidated under various conditions is listed in Table I.

Fig. 1 shows the XRD pattern of a typical $Mo_{\leq 5}Si_3C_{\leq 1}$ compact. It indicates that all peaks fit very well to the XRD pattern of $Mo_{4.8}Si_3C_{0.6}$ (PDF NO. 43-1199) and no peaks from other phases are present. Fig. 2 shows a typical microstructure of the compact. Although some SiO_2 phases existed, neither unreacted components nor other intermetallic phases were observed. The presence of SiO_2 would be due to a slight oxidation of the raw powders.

The B-$Mo_{45}Si_{30}C_5$ compact was synthesized at 1600°C–1700°C under 35 MPa for 1 to 2 hours. The compact consists of four phases of $Mo_{\leq 5}Si_3C_{\leq 1}$, MoB, $MoSi_2$ and SiC, as confirmed by SEM, EDS and XRD. The presence of four phases in B-$Mo_{\leq 5}Si_3C_{\leq 1}$ would be due to the phase equilibrium of the system. Although detailed thermodynamic investigations can not be accomplished due to the lack of thermodynamic data of the Mo-B phases in the Mo-Si-B-C system, this point can be confirmed by the relative experimental results and phase diagrams. The initial composition prior to hot pressing is $Mo_{0.530}Si_{0.354}B_{0.116}$ in the Mo-Si-B system when carbon is not counted. The ternary phase diagram of the Mo-Si-B system shows that BMo and $MoSi_2$ will appear by this composition at around 1600°C. Experiments [16] also confirmed that BMo and $MoSi_2$ coexisted with hot-pressed Mo_5Si_3 when the initial composition was $Mo_{0.556}Si_{0.334}B_{0.110}$. On the other hand, it becomes silicon-rich on the Mo-Si-C ternary system when MoB is formed; $MoSi_2$ and SiC thus form according to the equilibrium of the system. For example, the composition would be $Mo_{0.501}Si_{0.428}C_{0.071}$ if all the

TABLE I The density of various samples

Sample composition	Experimental conditions	Density (kg/m^3)
$Mo_{45}Si_{30}C_5$	HP at 1500°C for 1 h under 15 Mpa	7.28×10^3
$Mo_{45}Si_{30}C_5$	HP at 1700°C for 2 h under 15 Mpa	7.48×10^3
$Mo_{45}Si_{30}C_5$	HP at 1600°C for 1 h under 35 Mpa	7.56×10^3
$Mo_{45}Si_{30}C_5$	HP at 1700°C for 2 h under 35 Mpa	7.70×10^3
2 wt% Boron doped $Mo_{45}Si_{30}C_5$	HP at 1600°C for 1 h under 35 Mpa	7.47×10^3
2 wt% Boron doped $Mo_{45}Si_{30}C_5$	HP at 1700°C for 2 h under 35 Mpa	7.52×10^3
SiC-$Mo_{45}Si_{30}C_5$ composite	Infiltrated at 2100°C for 10 min.	4.35×10^3

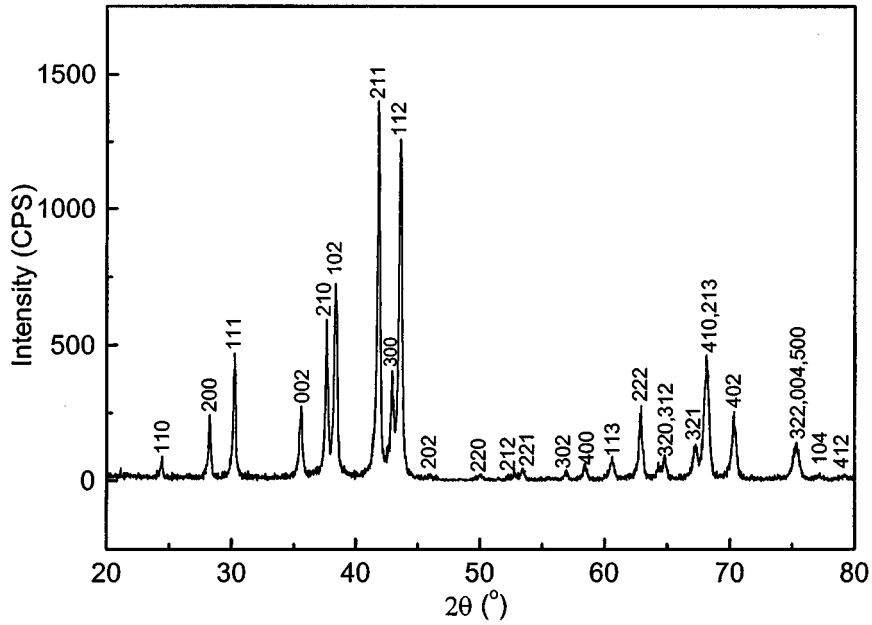

Figure 1 XRD pattern of a typical $Mo_{\leq 5}Si_3C_{\leq 1}$ compact hot-pressed at 1700°C for 2 h from raw powders of Mo, $MoSi_2$ and SiC. Tick marks are Bragg positions (PDF No. 43-1199).

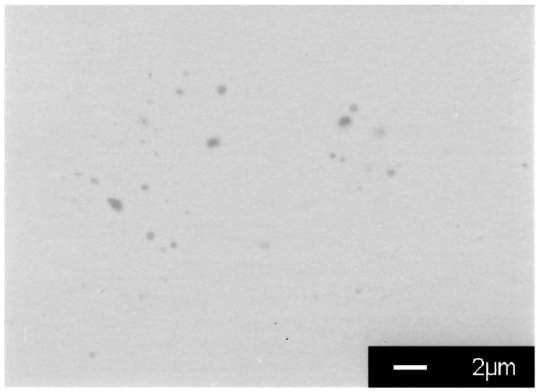

Figure 2 SEM micrograph of the polished surface of a $Mo_{\leq 5}Si_3C_{\leq 1}$ compact hot-pressed at 1700°C for 2 h. Black spots are SiO_2.

B were combined with Mo to form BMo. Although $Mo_{\leq 5}Si_3C_{\leq 1}$ was predicted to be a single phase over a broad composition range by the ternary Mo-Si-C phase diagram, it was found [14] that only in a narrow composition range, single-phase $Mo_{\leq 5}Si_3C_{\leq 1}$, was attainable by hot pressing at around 1600°C. The second phase will appear when the composition deviates from that range. Boron may slightly dissolve in the $Mo_{\leq 5}Si_3C_{\leq 1}$ phase, however, it is difficult to determine the amount by the current SEM/EDS system. The XRD pattern of a typical B-$Mo_{45}Si_{30}C_5$ is shown in Fig. 3. No peak from SiC was detected, indicating that the amount of SiC was very small.

SiC-$Mo_{\leq 5}Si_3C_{\leq 1}$ composites were fabricated at 2100°C by the melt infiltration process. Although

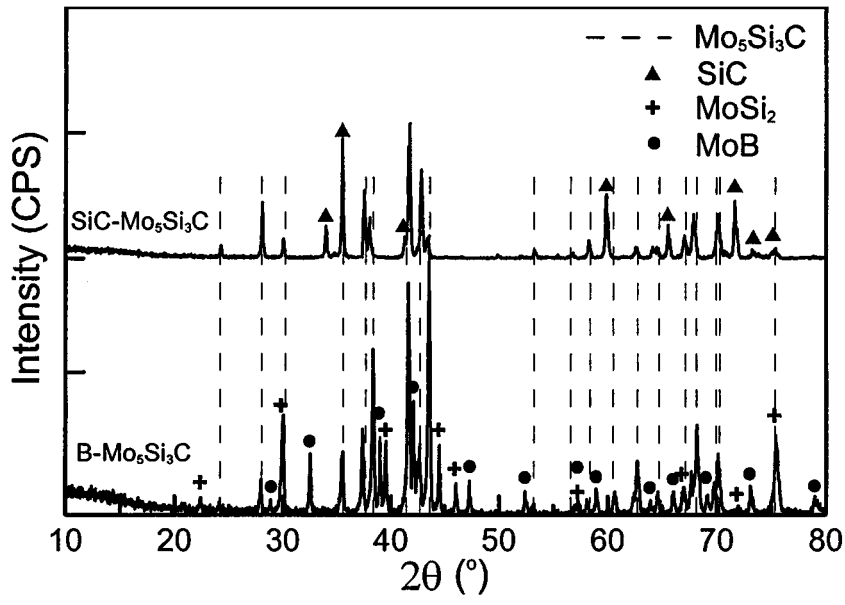

Figure 3 XRD patterns of SiC-$Mo_{\leq 5}Si_3C_{\leq 1}$ composites obtained from melt infiltration process at 2100°C for 10 min, and B-$Mo_{\leq 5}Si_3C_{\leq 1}$ compact hot-pressed at 1700°C for 2 h. The PDF numbers used are: $Mo_{\leq 5}Si_3C_{\leq 1}$ 43-1199; $MoSi_2$ 41-0612; MoB 06-0636 and SiC 29-1131.

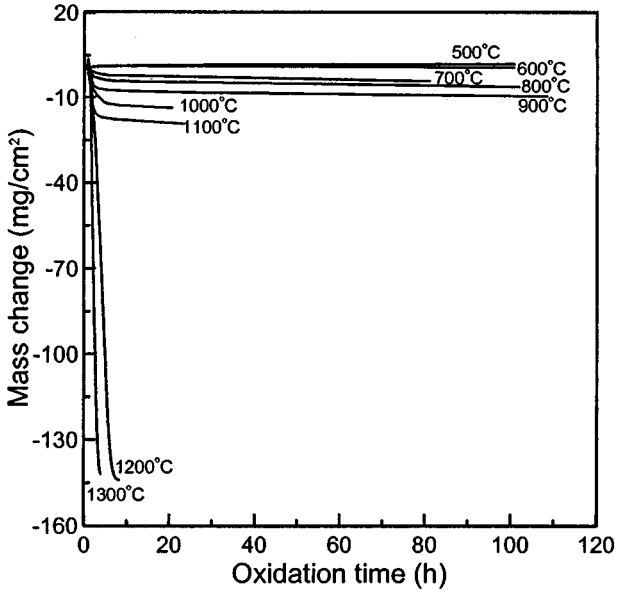

Figure 4 Oxidation-induced mass changes of $Mo_{\leq 5}Si_3C_{\leq 1}$ as a function of oxidation time in air at 500°C–1300°C. The specimens were completely oxidized within several hours at 1200°C and 1300°C.

10 min was adopted for infiltration, a few minutes was sufficient for full infiltration, indicating good wettability and low viscosity of the melt. The composite was almost fully dense, of a relative density greater than 95%, though there were some small uninfiltrated areas up to 10 μm randomly distributed in the microstructure. The composite was composed of SiC and $Mo_{\leq 5}Si_3C_{\leq 1}$ only, as exhibited by the XRD pattern in Fig. 3.

3.2. Oxidation of $Mo_{\leq 5}Si_3C_{\leq 1}$

The oxidation behavior of monolithic $Mo_{\leq 5}Si_3C_{\leq 1}$ was studied from 500°C to 1300°C. The oxidation-induced mass changes are plotted as a function of time in Fig. 4. These plots include the initial ramping stage up to the temperatures at 10°C/min. The mass change behavior during the initial stage at 800°C is replotted in Fig. 5. The overall oxidation reaction of the $Mo_{\leq 5}Si_3C_{\leq 1}$ phase would be as follows:

$$2Mo_5Si_3C + 23O_2 \rightarrow 10MoO_3 + 6SiO_2 + 2CO_2 \quad (1)$$

As seen from Fig. 5, the weight starts to increase at about 450°C, indicating that the oxidation becomes significant around 450°C. The weight gain is apparently due to the formation of MoO_3 and SiO_2, where, according to reaction (1), the weight change is a net gain of 56%. As the temperature increases, the weight continuously increases up to about 720°C. A quick weight loss was observed after 720°C, primarily due to the rapid volatilization of the MoO_3 phase. When MoO_3 completely volatilizes, reaction (1) indicates that the weight change is a net loss of 69%. As seen in Fig. 4, a continuous weight loss was observed during the holding stage at all temperatures except for that at 500°C and 600°C, where a small weight gain was obtained. The figure shows almost the same weight gain at 500°C and 600°C up to 40 h, indicating little difference in the oxidation rate at these temperatures. The weight gain is lower at 600°C above 40 h, probably due to the quick volatilization of MoO_3 at 600°C. As shown in Fig. 6, at 600°C the equilibrium vapor pressure of MoO_3(g), which is calculated from the thermodynamic data [17], is 150 times higher than that at 500°C. The oxidation rate increases with increasing temperature, and it dramatically increases when the oxidation temperature exceeds 1100°C. At 1300°C, the specimen was completely converted into powdery SiO_2 in less than 3 hours.

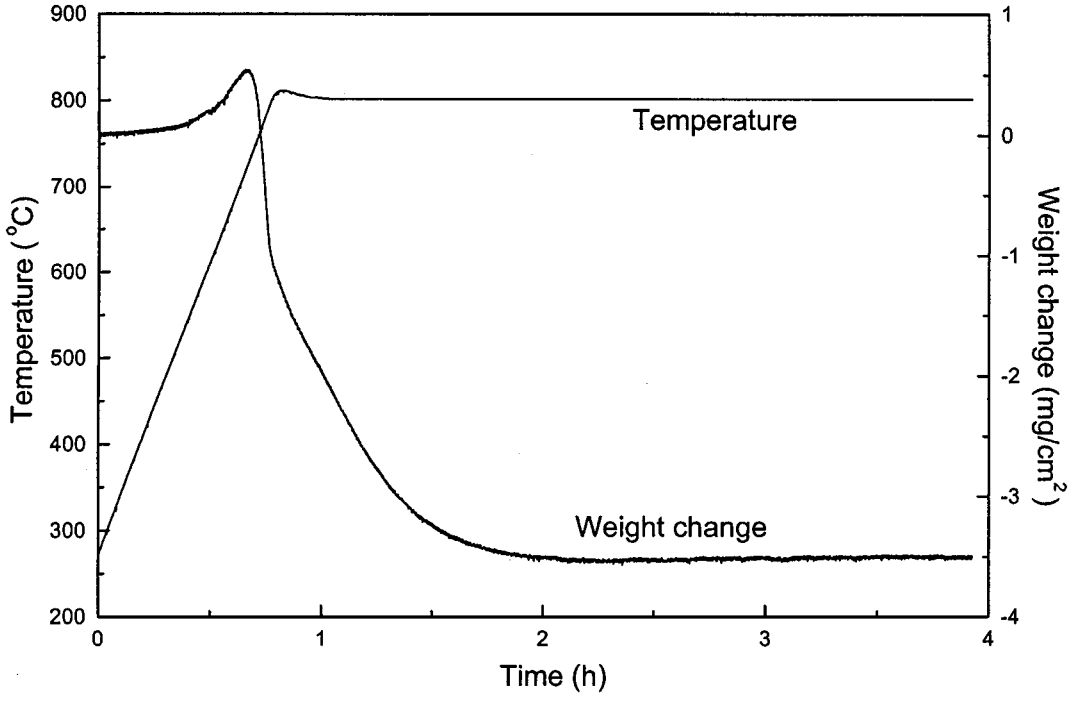

Figure 5 Mass change behavior of $Mo_{\leq 5}Si_3C_{\leq 1}$ during initial transient period. Initial mass gain is due to oxidation of $Mo_{\leq 5}Si_3C_{\leq 1}$, and the followed rapid weight loss is due to the volatilization of MoO_3.

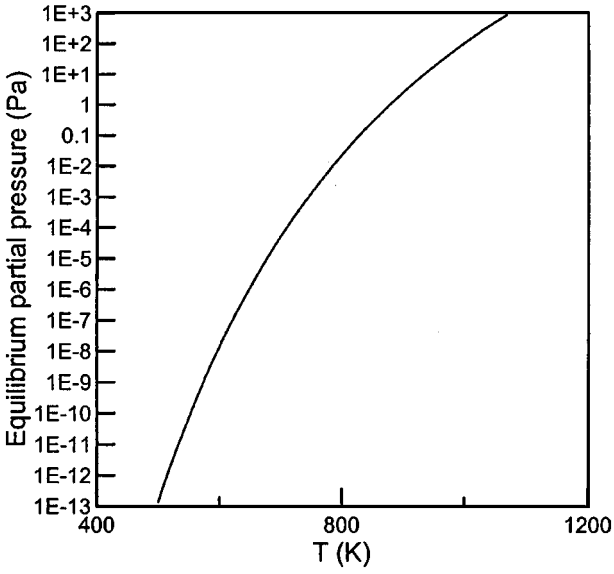

Figure 6 The equilirium partial pressure of MoO_3(g) vs. temperature. The equilibrium vapor pressure of MoO_3(g) at 600°C is 150 times higher than that at 500°C.

The oxidation behavior of $Mo_{\leq 5}Si_3C_{\leq 1}$ is similar to that of Mo_5Si_3 except that pest disintegration of the Mo_5Si_3 compact was reported at 800°C by Meyer and Akinc [16], while no pest disintegration was observed on $Mo_{\leq 5}Si_3C_{\leq 1}$ from 500°C to 900°C up to 100 h in the present study. MoO_3 volatilizes extensively above 720°C, so that above this temperature pest disintegration seems unlikely to occur because the volumetric mismatch associated with reaction (1) is small when MoO_3 volatilizes. We would, however, expect it at lower temperatures for an extended time like $MoSi_2$ [18]. At 500°C–600°C, the oxidized specimen was covered by a loose yellow-white scale, which was detected to be a mixture of MoO_3 and SiO_2, as indicated by the XRD patterns in Fig. 7. No peaks of SiO_2 were detected at 500°C–900°C, indicating that the SiO_2 formed at these temperatures is amorphous. The MoO_3 phase disappears on the oxidized surface above 900°C due to the quick volatilization of MoO_3. A large amount of white to yellow crystals with needlelike shape condensed on the cooler portion of the tube, which was examined by XRD to be MoO_3. The change of amorphous SiO_2 to cristobalite occurs at around 1000°C as shown by the XRD pattern. The powdery product at 1200°C–1300°C is cristobalite, and no other phases are found. As seen in Fig. 7, Mo_5Si_3, Mo_2C and Mo phases formed after oxidation at 900°C–1100°C. The formation of Mo_5Si_3, Mo_2C and Mo would be due to the selective oxidation of silicon in the interface of the oxide scale and the substrate. This point can be confirmed by the thermodynamic analyses given below.

The equilibrium of air (N_2 and O_2), CO, CO_2, SiO(g), MoO_2(g), MoO_3(g), MoO_3(l), $Mo_{\leq 5}Si_3C_{\leq 1}$, Mo_5Si_3, $MoSi_2$, Mo_3Si, MoC, Mo_2C, SiC, Mo, C (graphite), Si, SiO_2, MoO_2, MoO_3, Mo_4O_{11}, Mo_8O_{23}, and Mo_9O_{26} was studied by minimizing the free energy of the system [19]. All thermodynamic data were taken or calculated from references [17, 20, 21] except those of $Mo_{\leq 5}Si_3C_{\leq 1}$. $Mo_{\leq 5}Si_3C_{\leq 1}$ was considered as a line compound in the calculation. The free energy of $Mo_{\leq 5}Si_3C_{\leq 1}$ was based on the evaluation of Silva and Kaufman [11]. The thermodynamic calculations show that the oxidation of $Mo_{\leq 5}Si_3C_{\leq 1}$ simply proceeds

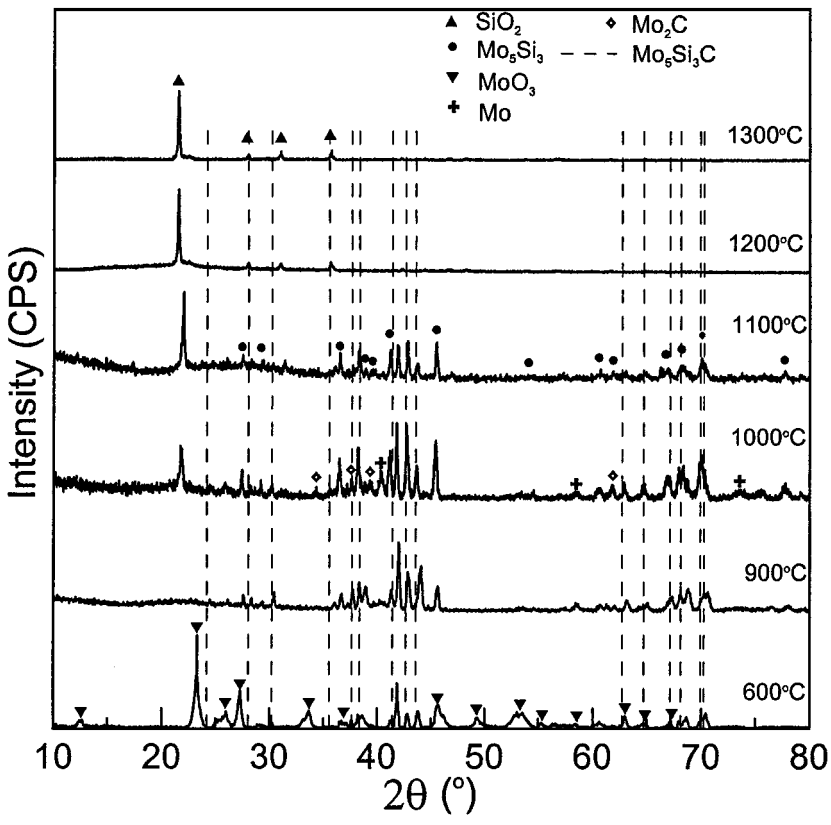

Figure 7 X-ray diffraction patterns of the oxidized surfaces of $Mo_{\leq 5}Si_3C_{\leq 1}$. Oxidation times are indicated in Fig. 4. The PDF numbers used are: $Mo_{\leq 5}Si_3C_{\leq 1}$ 43-1199; Mo_5Si_3 34-0371, Mo 42-1120; SiO_2 39-1425; MoO_3 05-0508 and Mo_2C 31-0871.

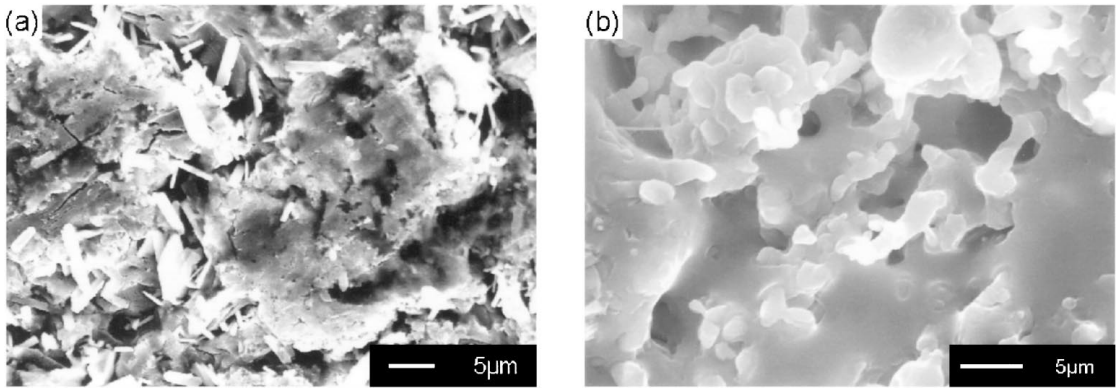

Figure 8 SEM micrographs of the oxidized surfaces of $Mo_{\leq 5}Si_3C_{\leq 1}$ after oxidation in air at: (a) 600°C for 100 h, (b) 900°C for 108 h.

according to reaction (1) when the oxygen is sufficient. However, if the oxygen is insufficient, the oxidation of $Mo_{\leq 5}Si_3C_{\leq 1}$ becomes complicated as indicated by reaction (2). The parameters of x, y, z, $x1$ and $x2$ depend on the oxidation conditions (like oxygen partial pressure, temperature, *et al.*). From the thermodynamic point of view, the oxygen tends to combine with the silicon to form SiO_2 during oxidation in an oxygen-lean environment, because the free energy of SiO_2 is much smaller than that of the other oxides. The relative amount of Mo_5Si_3, Mo_2C and Mo can be determined through minimizing the free energy of the system.

$$Mo_5Si_3C + xO_2 \rightarrow yMo_5Si_3 + zMo_2C + x1Mo + x2SiO_2 \quad (2)$$

Calculations show that the oxidation of Mo_5Si_3 can be expressed by reactions (3) and (4), depending on the oxidation atmosphere. Reaction (3) is preferred in an excessive oxygen environment, while the preferential oxidation of silicon occurs in an oxygen-lean environment as indicated by reaction (4). The oxidation of Mo_2C would occur according to reactions (5) and (6), depending on the oxidation temperature and atmosphere. The selective oxidation of carbon is thermodynamically preferred in an oxygen-lean environment only when the oxidation temperature is above ~1200 K; otherwise, the selective oxidation does not take priority. Mo will finally be oxidized according to reaction (7).

$$2Mo_5Si_3 + 21O_2 \rightarrow 10MoO_3 + 6SiO_2 \quad (3)$$

$$Mo_5Si_3 + 3O_2 \rightarrow 5Mo + 3SiO_2 \quad (4)$$

$$Mo_2C + 4O_2 \rightarrow 2MoO_3 + CO_2 \quad (5)$$

$$2Mo_2C + O_2 \rightarrow 4Mo + 2CO \quad (6)$$

$$2Mo + 3O_2 \rightarrow 2MoO_3 \quad (7)$$

The thermodynamic studies are in good agreement with the oxidation behavior of $Mo_{\leq 5}Si_3C_{\leq 1}$ and the oxidation of Mo_5Si_3 and $MoSi_2$ [22–24], which revealed the formation of a molybdenum-rich layer between the oxide scale and the substrate. During the initial oxidation period which starts at ~450°C, $Mo_{\leq 5}Si_3C_{\leq 1}$ must be fully oxidized to form CO_2, SiO_2 and MoO_3 because there is sufficient oxygen. The oxide scale formed during oxidation at low temperatures (450°C–700°C) would be the mixture of SiO_2 and MoO_3, and the scale is porous in general as indicated by Fig. 8a. MoO_3 volatilizes at a higher temperature, leaving a porous SiO_2 network. Although this porous SiO_2 layer could become denser through a viscous sintering mechanism, the temperature would be too low to obtain rapid sintering to effectively close the pores. Also, the amount of volatile material (MoO_3 and CO_2) would be too great to close these pores easily as compared to the case of $MoSi_2$ oxidation. Fig. 8b shows a typical oxide scale of the long time oxidation. It shows that pores still exist after oxidation for more than 100 h at 900°C. Further oxidation of the substrate proceeds through the diffusion of reactants and oxidation products through this SiO_2 layer. The overall oxidation rate may be limited by the diffusion of oxygen through the gas boundary layer and the oxide scale, or by the governing reaction, or by the diffusion of oxidation products out through the oxide scale and the gas boundary layer. If the oxidation is limited by the governing reaction or by the transfer of the oxidation products, the partial pressure of oxygen must be higher than the equilibrium partial pressure at the interface of the oxide scale and the substrate, and therefore, selective oxidation will not occur. A molybdenum-rich interlayer was actually formed, indicating that oxygen transportation is rate-limiting. The reaction rate increases with increasing temperature. At 1200°C and above, the rapid oxidation of $Mo_{\leq 5}Si_3C_{\leq 1}$ produces a large amount of MoO_3(g) and CO_2, which makes it more difficult to reduce the porosity of the oxide scale through viscous sintering. The porous scale of SiO_2 provides little diffusion barrier of oxygen, resulting in poor oxidation resistance of the material at high temperature.

Above 720°C, reaction (1), (3) and (5)–(7) result in a net weight loss, while other reactions generate a net weight gain. The weight-change data in Fig. 4 reveal that a net weight loss was observed together with the formation of Mo and Mo_5Si_3 phases, indicating that the weight-loss reactions dominate the whole process.

3.3. Oxidation of B-$Mo_{\leq 5}Si_3C_{\leq 1}$

The addition of 2 wt% boron greatly improves the oxidation resistance of the $Mo_{\leq 5}Si_3C_{\leq 1}$ phase. The mass change behavior of B-$Mo_{\leq 5}Si_3C_{\leq 1}$ from 600°C

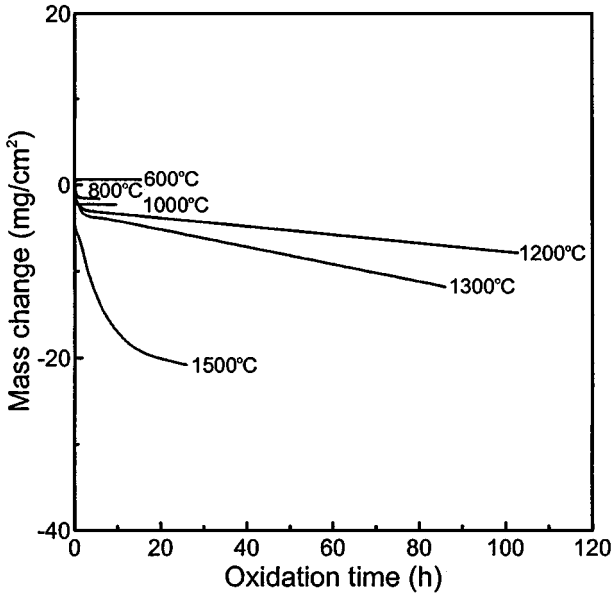

Figure 9 Mass changes of B-$Mo_{\leq 5}Si_3C_{\leq 1}$ as a function of oxidation time in air at 600°C–1500°C.

to 1500°C is shown in Fig. 9. The oxidation behavior of B-$Mo_{\leq 5}Si_3C_{\leq 1}$ in the ramping stage is similar to that of $Mo_{\leq 5}Si_3C_{\leq 1}$ and is not shown in the figure. As seen in Fig. 9, the oxidation behavior of B-$Mo_{\leq 5}Si_3C_{\leq 1}$ is similar to that of $Mo_{\leq 5}Si_3C_{\leq 1}$ between 600°C and 1000°C, except that the oxidation rate is much lower in the case of B-$Mo_{\leq 5}Si_3C_{\leq 1}$. A big improvement in the oxidation resistance was found at high temperatures (1200°C–1500°C). The oxidation rate slows by an order of magnitude after oxidizing for 100 h at 1200°C, comparing the complete oxidation of $Mo_{\leq 5}Si_3C_{\leq 1}$ within several hours. The steady-state oxidation was observed at 1200°C–1500°C after the initial rapid weight loss. A black scale formed after oxidation, in contrast to the white scale formed on undoped $Mo_{\leq 5}Si_3C_{\leq 1}$. The oxidized scale is a mixture of MoO_3, SiO_2 and B_2O_3 at 600°C–800°C, confirmed by XRD and EDS. The XRD patterns of the oxidized surfaces are shown in Fig. 10. No peak of B_2O_3 was observed on the oxide scale, indicating that the B_2O_3 formed was amorphous. The SiO_2 formed at 1200°C–1500°C was cristobalite, while it was amorphous at the other temperatures. The figure clearly shows the formation of Mo_5Si_3, Mo_2C and Mo phases at 1000°C–1300°C, suggesting that the selective oxidation of silicon occurred in the interface of oxidation, primarily due to the same mechanism as previously noted. The oxidation behavior of B-$Mo_{\leq 5}Si_3C_{\leq 1}$ is more complicated than that of $Mo_{\leq 5}Si_3C_{\leq 1}$, because B-$Mo_{\leq 5}Si_3C_{\leq 1}$ is the mixture of $Mo_{\leq 5}Si_3C_{\leq 1}$, $MoSi_2$, SiC and MoB. Although thermodynamic investigations of the oxidation of B-$Mo_{\leq 5}Si_3C_{\leq 1}$ could not be accomplished due to the lack of thermodynamic data of the Mo-B phases, the oxidation behavior of SiC and $MoSi_2$ are well established experimentally and thermodynamically [22–26]. The oxidation of SiC would be active (reaction 8) or passive (reaction 9), depending on the oxygen partial pressure and the temperature. The oxidation of $MoSi_2$ in oxygen-lean environments shows the selective oxidation of silicon, as indicated by reaction (10). The oxidation path of MoB is not very clear, and the overall oxidation reaction of the MoB phase could be expressed as reaction (11).

$$SiC + O_2 \rightarrow SiO(g) + CO \quad (8)$$

$$2SiC + 3O_2 \rightarrow 2SiO_2 + 2CO \quad (9)$$

$$5MoSi_2 + 7O_2 \rightarrow Mo_5Si_3 + 7SiO_2 \quad (10)$$

$$4MoB + 9O_2 \rightarrow 4MoO_3 + 2B_2O_3 \quad (11)$$

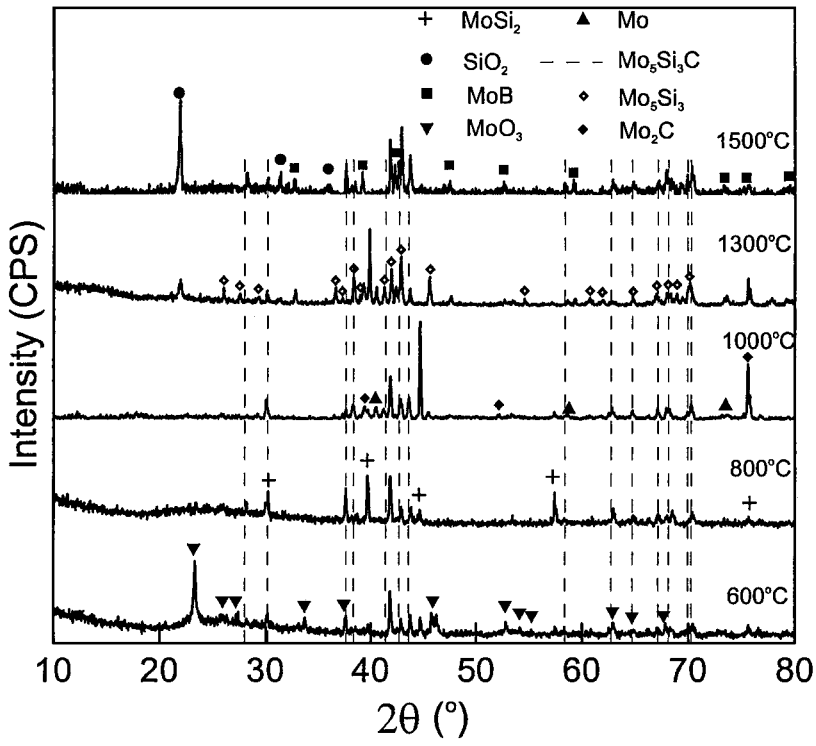

Figure 10 XRD patterns of the oxidized surfaces of B-$Mo_{\leq 5}Si_3C_{\leq 1}$ composite after oxidation at 600°C–1500°C. Oxidation times are shown in Fig. 9. The PDF numbers used are: $Mo_{\leq 5}Si_3C_{\leq 1}$ 43-1199; Mo_5Si_3 34-0371, Mo 42-1120; SiO_2 39-1425; MoO_3 05-0508; Mo_2C 31-0871; $MoSi_2$ 41-0612 and MoB 06-0636.

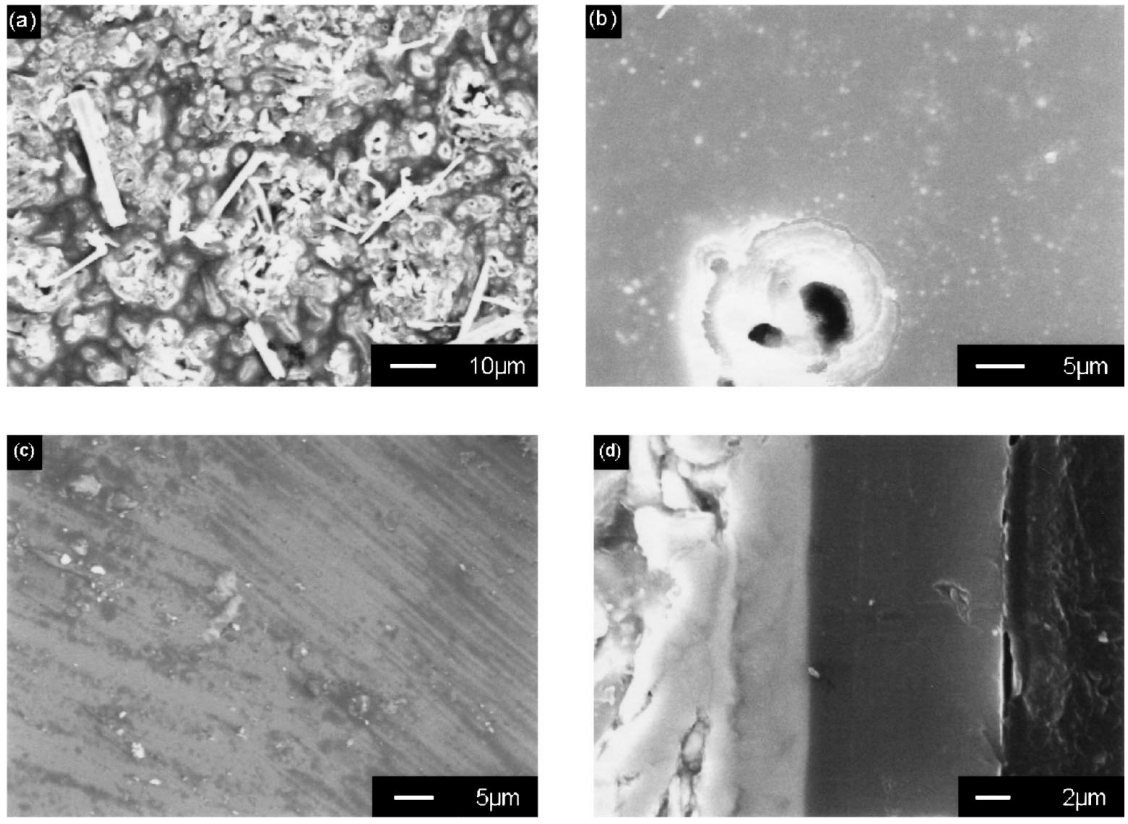

Figure 11 SEM micrographs of oxide scale formed on B-$Mo_{\leq 5}Si_3C_{\leq 1}$ after oxidation in air at: (a) 600°C for 15 h, (b) 1000°C for 10 h, (c) 1500°C for 24 h (oxidized surface), (d)1500°C for 24 h (cross section). Micrograph in (d) shows left to right, oxidation specimen, oxide scale and resin binder used to secure sample.

The scale initially formed as a mixture of borosilicate glass and MoO_3(s), and it is porous as exhibited by Fig. 11a. MoO_3(s) volatilizes extensively above 720°C, leaving a porous borosilicate glass scale. With the aid of B_2O_3, the porous scale can be easily densified, compared with the case of undoped $Mo_{\leq 5}Si_3C_{\leq 1}$. As seen in Fig. 11b, denser scales with pores here and there formed after oxidation at 1000°C for 10 h. No through-scale porosity was found by SEM after oxidation at 800°C–1100°C. The pores may result from the volatilization of MoO_3 and B_2O_3, which have a high vapor pressure at these temperatures. Small pores in the scale provide short-circuit paths for oxygen transport to the oxidation interface, and quick oxidation occurs at the areas near the pores. At higher temperatures and longer times, these pores can be closed through the viscous sintering mechanism. SEM observations confirmed that dense scales without pores and cracks formed after oxidizing at 1200°C–1500°C, as exhibited by Fig. 11c and d. The improvement in oxidation resistance provided by boron addition is obviously attributed to the formation of a dense oxide scale, which provides a good diffusion barrier of oxygen at high temperatures.

The oxidation behavior of B-$Mo_{\leq 5}Si_3C_{\leq 1}$ is similar to that of B-Mo_5Si_3 which is a mixture of Mo_5Si_3, MoB and $MoSi_2$ [16], except that weight gain was observed between 1050°C and 1300°C in the case of B-Mo_5Si_3. Although weight gain is associated with the formation of Mo_5Si_3 and Mo phases, Mo can come out of the dense oxidized film through diffusion, concurrently with the formation of Mo, and the subsequent oxidation of Mo may cause a net weight loss. Weight loss was also observed with the formation of the Mo phase in the oxidation of B-Mo_5Si_3 at 800°C–1000°C [16], where a dense oxide scale formed and the strongest peaks of Mo were detected by XRD. It should be noted that the real path of oxidation must depend on experimental conditions, such as the surface topography of the oxide, temperature, pressure and the flow pattern. Therefore, the observation of a net weight gain or weight loss should be very sensitive to precise experimental conditions.

3.4. Oxidation of SiC-$Mo_{\leq 5}Si_3C_{\leq 1}$ composite

Oxidation tests have been also conducted on SiC-$Mo_{\leq 5}Si_3C_{\leq 1}$ composites at 800°C, 1300°C and 1600°C. The isothermal mass changes of the composite are shown in Fig. 12. A small weight loss was observed during the initial period of oxidation, due to the volatilization of MoO_3 caused by the oxidation of the $Mo_{\leq 5}Si_3C_{\leq 1}$ phases. After the initial stage, the weight of the samples slowly increases, and the oxidation behavior of the composite turns into passive oxidation. The oxidation resistance of the composite at 1600°C is fairly good and is comparable to that of the SiC film [27]. Fig. 13 shows the micrographs of the oxidized surface at 800°C and 1300°C. The bright phases in the microstructure of Fig. 13a are detected to be SiO_2, which may result from the oxidation of the $Mo_{\leq 5}Si_3C_{\leq 1}$ phases. A dense SiO_2 layer with micro cracks formed after oxidation at 1300°C for 100 h, as exhibited by Fig. 13b. The micro-cracks on the oxide film probably result from thermal expansion differences between the substrate and the silica layer that put the film in tension on cooling [28]. The XRD patterns in Fig. 14 show that

the silica formed at 1300°C is a cristobalite. The peaks of the Mo_2C, Mo_5Si_3 and Mo phases, which are due to the partial oxidation of the $Mo_{\leq 5}Si_3C_{\leq 1}$ phases, were also found in the XRD pattern.

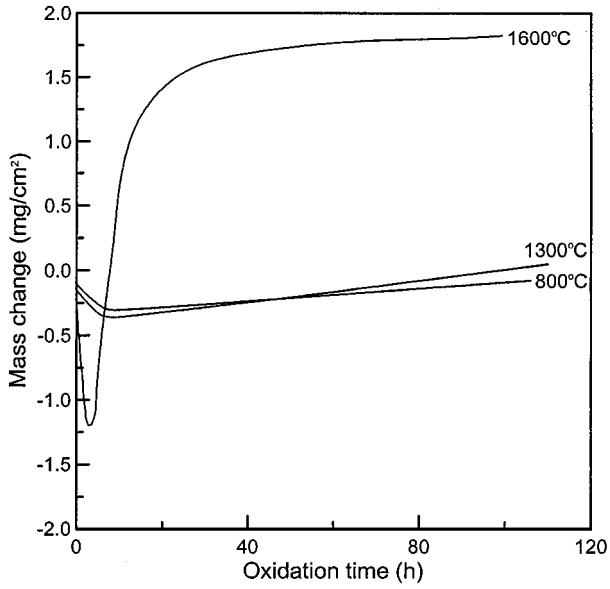

Figure 12 Mass changes of SiC-$Mo_{\leq 5}Si_3C_{\leq 1}$ composite as a function of oxidation time in air at 800°C, 1300°C and 1600°C.

4. Conclusions

The oxidation resistance of $Mo_{\leq 5}Si_3C_{\leq 1}$-based materials was investigated in the present study. Monolithic $Mo_{\leq 5}Si_3C_{\leq 1}$ and B-$Mo_{\leq 5}Si_3C_{\leq 1}$ composite were synthesized by hot pressing from raw powders of Mo, SiC, $MoSi_2$ and B. SiC-$Mo_{\leq 5}Si_3C_{\leq 1}$ composite was fabricated through melt infiltration process at 2100°C.

The oxidation resistance of monolithic $Mo_{\leq 5}Si_3C_{\leq 1}$ was tested from 500°C to 1300°C. Monolithic $Mo_{\leq 5}Si_3C_{\leq 1}$ compact exhibits poor oxidation resistance at 1200°C and above. The specimens were completely oxidized into powdery SiO_2 within several hours at these temperatures. A mixed SiO_2-MoO_3 oxide initially forms, covering the surface of the specimen. At approximately 720°C, MoO_3 quickly volatilizes, leaving a porous layer of SiO_2. The pores in the layer are difficult to close entirely by viscous sintering mechanism due to the low temperature and the volatilization of MoO_3. The porous scale of SiO_2 provides little diffusion barrier of oxygen, resulting in poor oxidation resistance of the material at high temperatures. Thermodynamic simulations demonstrated that the selective oxidation of silicon in $Mo_{\leq 5}Si_3C_{\leq 1}$ was preferred during oxidation in an oxygen-lean environment. Mo_5Si_3, Mo and Mo_2C phases thus formed due to this selective oxidation. The calculated results are in good agreement

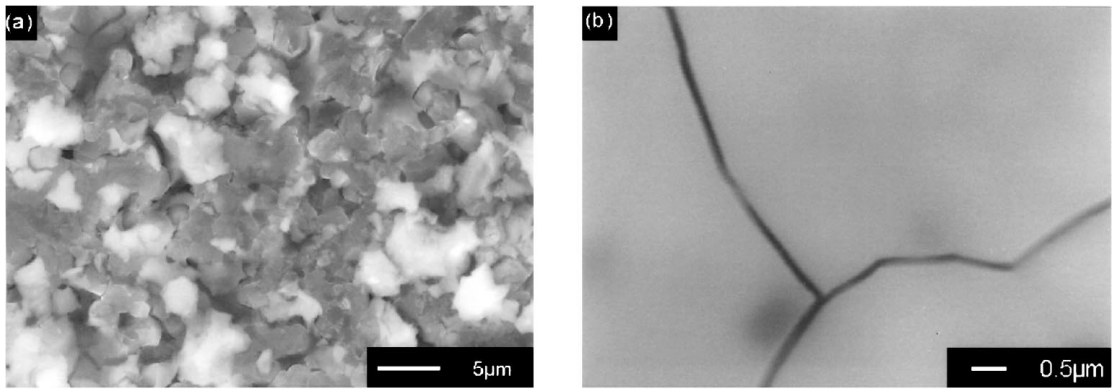

Figure 13 The surface morphologies of SiC-$Mo_{\leq 5}Si_3C_{\leq 1}$ composites after oxidation in air at: (a) 800°C for 106 h and (b) 1300°C for 110 h. The bright phases in (a) are SiO_2 and the dark phases are detected to be SiC by EDS.

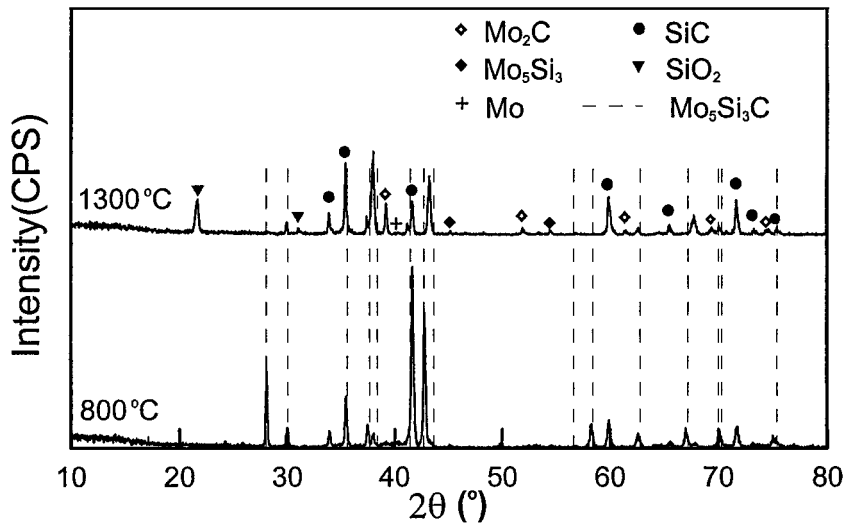

Figure 14 XRD patterns of the oxide scale of SiC-$Mo_{\leq 5}Si_3C_{\leq 1}$ composite after oxidation at 800°C for 106 h and 1300°C for 110 h. The PDF numbers used are: $Mo_{\leq 5}Si_3C_{\leq 1}$ 43-1199; Mo_5Si_3 34-0371, Mo 42-1120; SiO_2 39-1425; Mo_2C 31-0871 and SiC 29-1131.

with the experimental data, which showed the formation of Mo_5Si_3, Mo_2C and Mo phases.

In order to improve the oxidation resistance of the $Mo_{\leq 5}Si_3C_{\leq 1}$ phase, boron was added to the $Mo_{\leq 5}Si_3C_{\leq 1}$ phase. The addition of 2 wt% boron produced a composite with three other phases of $MoSi_2$, MoB and SiC, which showed remarkable improvement in oxidation resistance. The pores which resulted from the volatilization of MoO_3, could be easily closed to form a dense layer of SiO_2 through the viscous sintering mechanism with the aid of B_2O_3. A dense layer of SiO_2 formed after oxidation at 1200°C–1500°C. The improvement in the oxidation resistance provided by boron addition is attributed to the formation of a dense oxide scale, which provides a good diffusion barrier of oxygen at high temperature. The selective oxidation of silicon also occurred in the interface between the oxide scale and the substrate.

The oxidation tests were also conducted on SiC-$Mo_{\leq 5}Si_3C_{\leq 1}$ composites at 800°C, 1300°C and 1600°C for more than 100 h. There is slight weight loss during the initial oxidation period due to the volatilization of the MoO_3 phase. After this initial stage, passive oxidation was observed. The oxidation resistance of the SiC-$Mo_{\leq 5}Si_3C_{\leq 1}$ composite is fairly good. A dense oxide film formed after oxidation at 1300°C and 1600°C for 100 h.

References

1. K. UPADHYA, J.-M. YANG and W. P. HOFFMAN, *Amer. Ceram. Soc. Bull.* **76** (1997) 51.
2. P. J. MESCHTER and D. S. SCHWARTZ, *JOM* **41** (1989) 52.
3. J.-P. HIRVONEN, P. TORRI, R. LAPPALAINEN, J. LIKONEN, H. KUNG, J. R. JERVIS and M. NASTASI, *J. Mater. Res.* **13** (1998) 965.
4. K. ITO, T. YANO, T. NAKAMOTO, M. MORIWAKI, H. INUI and M. YAMAGUCHI, *Progress in Materials Science* **42** (1997) 193.
5. S. BOSE, *Mater. Sci. Eng.* **A155** (1992) 217.
6. A. K. VASUDEVAN and J. J. PETROVIC, *ibid.* **A155** (1992) 1.
7. H. NOWOTNY, E. PARTHE, R. KIEFFER and F. BENESOVSKY, *Monatsh. Chem.* **85** (1954) 255.
8. E. PARTHE, W. JEITSCHKO and V. SADAGOPAN, *Acta Crystallogr.* **19** (1965) 1031.
9. L. BREWER and O. KRIKORIAN, *J. Electrochem. Soc.* **85** (1956) 38.
10. F. J. J. VAN LOO, F. M. SMET, G. D. RIECK and G. VERSPUI, *High Temp.-High Press.* **14** (1982) 25.
11. A. COSTAe SILVA and M. J. KAUFMAN, *Metall. Mater. Trans.* **25A** (1994) 5.
12. S. MALOY, A. H. HEUER, J. LEWANDOWSKI and J. PETROVIC, *J. Amer. Ceram. Soc.* **74** (1991) 2704.
13. S. MALOY, J. J. LEWANDOWSKI, A. H. HEUER and J. J. PETROVIC, *Mater. Sci. Eng.* **A155** (1992) 159.
14. Y. SUZUKI and K. NIIHARA, *Intermetallics* **6** (1998) 7.
15. R. RAJ, *J. Amer. Ceram. Soc.* **76** (1993) 2147.
16. M. K. MEYER and M. AKINC, *ibid.* **79** (1996) 938.
17. M. W. CHASE, JR., C. W. DAVIES, J. R. DOWNEY, JR., D. J. FRURIP, R. A. MCDONALD and A. N. SYVERUD, *JANAF Thermochemical Tables*, 3rd ed. (American Chemical Society, New York, 1985). J. Phys. Chem. Vol. 14, Suppl. 1. (Ref. Data).
18. T. C. CHOU and T. G. NIEH, *J. Mater. Res.* **8** (1993) 214.
19. W. B. WHITE, S. M. JOHNSON and G. B. DANTZIG, *J. Chem. Phys.* **28** (1958) 751.
20. D. R. STULL and H. PROPHET, *JANAF Thermochemical Tables*, 2nd ed. (Washington, 1971).
21. I. BARIN, F. SAUERT, E. SCHULTZE-RHONHOF and S. S. WANG, *Thermochemical Data of Pure Substance*, Federal Republic of Germany, 1993.
22. J. B. BERKOWITZ-MATTUCK and R. R. DILS, *J. Electrochem. Soc.* **112** (1965) 583.
23. A. W. SEARCY, *J. Amer. Ceram. Soc.* **40** (1957) 431.
24. R. W. BARTLETT, J. W. MCCAMONT and P. R. GAGE, *ibid.* **48** (1965) 551.
25. Q. S. ZHU, X. L. QIU and C. W. MA, *Computers & Applied Chemistry* **13** (1996) 91.
26. T. NARUSHIMA, T. GOTO, Y. IGUCHI and T. HIRAI, *J. Amer. Ceram. Soc.* **74** (1991) 2583.
27. Q. S. ZHU, X. L. QIU and C. W. MA, *J. Nucl. Mater.* **254** (1998) 221.
28. D. S. FOX, *J. Amer. Ceram. Soc.* **81** (1998) 945.

Received 10 February
and accepted 11 August 1999